Journal of Power Sources 230 (2013) 32–37

Contents lists available at SciVerse ScienceDirect

Journal of Power Sources

journal homepage: www.elsevier.com/locate/jpowsour

In situ high-energy X-ray diffraction to study overcharge abuse of 18650-size lithium-ion battery

Chi-Kai Lin [a,*], Yang Ren [b], Khalil Amine [a], Yan Qin [a], Zonghai Chen [a]

[a] Chemical Sciences and Engineering Division, Argonne National Laboratory, 9700 South Cass Avenue, Argonne, IL 60439-4837, USA
[b] X-Ray Science Division, Argonne National Laboratory, 9700 South Cass Avenue, Argonne, IL 60439-4837, USA

HIGHLIGHTS

- A new application of *in situ* high-energy X-ray diffraction.
- The contribution of anodes and cathodes in an overcharged 18650 lithium-ion cell is determined.
- The temperature of the cathode begins to increase at a lower voltage than that of the anode.
- The electrochemical stability of the delithiated cathode plays a more critical role than the anode.

ARTICLE INFO

Article history:
Received 27 September 2012
Received in revised form
28 November 2012
Accepted 6 December 2012
Available online 13 December 2012

Keywords:
Overcharge abuse
In situ high-energy X-ray diffraction
Lithium-ion battery
Phase transition
$LiNi_{0.8}Co_{0.15}Al_{0.05}O_2$ cathode

ABSTRACT

Overcharge is an aggressive abuse condition that can lead to thermal runaway of a lithium-ion cell. Understanding the failure mechanism due to overcharge is critical for designing safer lithium-ion chemistries. With the help of *in situ* high-energy X-ray diffraction (XRD), we are able to detect the temperature difference between the cathode and the anode during the overcharge abuse of 18650 cells. In this paper, the lattice constants of electrode current collectors (Al for the cathode and Cu for the anode) are calculated by fitting the XRD patterns, and the temperature variations of the cathode and anode are quantified by the thermal expansion of the Al and Cu foils. Based on these results, we report that during the overcharge abuse of an 18650-size cell, using graphite as the anode and $LiNi_{0.8}Co_{0.15}Al_{0.05}O_2$ as the cathode, the temperature of cathode increases as the voltage reaches 4.16 V, corresponding to the occurrence of the H2-to-H3 phase transition in the cathode material.

1. Introduction

Lithium-ion batteries, a promising clean-energy carrier and storage technology, have long been pursued for application in hybrid electric vehicles, plug-in hybrid electric vehicles, and electric energy storage for grid applications [1,2]. However, use of lithium-ion batteries for these applications raises safety concerns because they may rupture, catch fire, or explode. These problems have long been blamed on exothermic reactions between battery components, such as unwanted chemical reactions between delithiated cathodes or lithiated anodes and non-aqueous electrolytes [3–6]. Part of the heat generated by these reactions dissipates through the battery to the environment, but locally accumulated heat induces other exothermic reactions, leading to the catastrophic failure of the battery by thermal runaway [7,8]. Many battery fires and explosions reported during the past years have been ascribed to overheated batteries, both in mobile phones and electric vehicles [9]. Therefore, a substantial amount of research has been performed to improve the tolerance to thermal abuse [3–6] and heat dissipation rate of these batteries [10,11].

Several tests are widely used to characterize the abuse tolerance of batteries, including nail penetration, external short circuit tests, oven tests, and overcharge tests [12,13]. These testing procedures screen batteries effectively but provide little detailed information about the failure mechanism. Since the battery is a complex system, the contribution of each component to battery safety needs to be addressed.

Conventional surface-mounted thermocouples measure the temperature of the external battery case, which is much lower than the internal temperature [14,15], and thus determine only the total dissipated heat. Although placing thermocouples directly on the

* Corresponding author. Tel.: +1 630 252 6445; fax: +1 630 972 4525.
E-mail addresses: chikai.moses.lin@gmail.com, cklin@anl.gov (C.-K. Lin), ren@aps.anl.gov (Y. Ren), amine@anl.gov (K. Amine), qin@anl.gov (Y. Qin), zonghai.chen@anl.gov (Z. Chen).

0378-7753/$ – see front matter © 2012 Elsevier B.V. All rights reserved.
http://dx.doi.org/10.1016/j.jpowsour.2012.12.032

electrodes can measure the temperature change in real time, this invasive method is still not able to distinguish exothermic reactions at different battery components, since limited space between the cathode and the anode makes it difficult to insert more than one thermocouple. Attempts to tackle this limitation by extracting temperature information from a specific component based on its unique intrinsic properties have met with limited success. For example, Srinivasan [16] reported use of a four-probe electrical technique to explore the relationship between the temperature of the solid–electrolyte interface (SEI) and the impedance of the anode. However, this method only monitors the anode temperature and only works at temperatures below 70 °C because of the decomposition temperature of the SEI (80–120 °C) [17]. Therefore, advanced techniques are still needed to identify the specific contribution of each component in working batteries to their tolerance to abuse.

Taking advantage of the fact that cathode and anode materials are coated on different current collectors (Al and Cu foils, respectively) in the standard lithium-ion battery, we propose here that the temperature variation of the electrodes can be differentiated by analyzing the thermal expansion of the lattice constants of Al and Cu. To prove this concept, we applied *in situ* high-energy X-ray diffraction (XRD) to 18650-size cells during overcharge abuse to identify the failure mechanism of the lithium-ion battery.

Previous studies have reported several undesirable possibilities when a lithium-ion battery undergoes overcharge. First, the anode loses stability, because it becomes a reducing agent as electrons are continually injected into the anode, and the excess lithium ions cause metallic lithium deposition on the anode [18]. Second, the cathode loses stability, because it becomes an oxidizing agent as electrons are continually extracted from it [19]. Third, the battery temperature is elevated by the reactions of unstable electrodes with electrolytes and by resistive heating (I^2R) [20]. Fourth, the temperature and cell pressure rise due to these reactions, further causing thermal runaway with cell rupture [21]. However, the true failure mechanism for overcharging a lithium-ion battery depends strongly on various physical conditions, such as the cathode-to-anode (C/A) ratio, the chemistry of the electrode materials, and the thermal dissipation efficiency of the cells or pack. It is not well understood if anode instability, cathode instability, or resistive heating is the origin of the exothermic process. Understanding the true failure mechanism is critical for the design of safer lithium-ion chemistry with better tolerance of overcharge abuse.

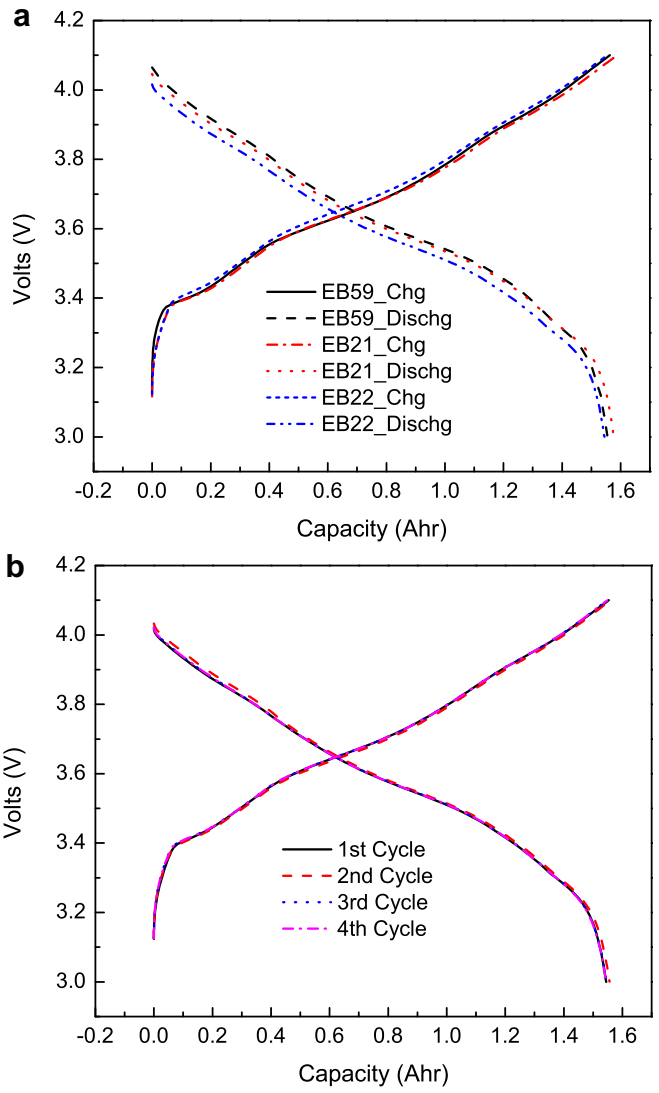

Fig. 1. Electrochemical curves of 18650 cells. (a) Charge–discharge profiles of EB21, 22, and 59. (b) Profiles of first to fourth cycles of EB21.

2. Experimental

2.1. 18650 cells investigated

A series of cylindrical 18650 lithium-ion cells was fabricated with an anode of mesocarbon microbeads, electrolyte of 1.2 M $LiPF_6$ with ethylene carbonate and ethyl methyl carbonate (weight ratio of 3:7), and cathode of $LiNi_{0.8}Co_{0.15}Al_{0.05}O_2$ (NCA). The anode-to-cathode ratio was 1.2, and the separator was a microporous polyethylene membrane, Celgard® 2325. The total weight of an 18650 cell is about 40 g, and the reversible capacity of each cell is around 1.6 Ah. Fig. 1a shows charge–discharge curves of several 18650 cells (EB21, 22, and 59) cycled between 3.0 V and 4.1 V using a constant current of 0.18 A (C/10). Fig. 1b shows an exemplary charge–discharge profile, with good capacity and voltage retention.

2.2. Safety guard

A safety guard was carefully designed for the *in situ* XRD to handle possible safety concerns as the lithium-ion cell undergoes overcharge. A diagram of the safety guide with multiple views is given in Fig. 2. The inner view (Fig. 2b) shows a cell holder (the black case) for standard 18650 cells. The plastic cell holder has two electrical contacts, which are connected to an external Maccor® battery tester, and an electric insulator plate, which is inserted between the bottom surface of the stainless-steel housing and the plastic cell holder. The top of the stainless-steel box is locked to the bottom plate with four screws. Two windows (diameter of 1 in. for diffracted X-rays and ¼ in. for incident X-rays) are opened in the light path of the diffracted and incident X-rays to reduce unnecessary background from the safety box. Both of the windows are sealed with Kapton® films to reduce gas leakage in case of cell rupture. An Ar flow can be switched on to protect the battery, and an exhaust vent is installed to remove any gas released from the cell (Fig. 2c).

2.3. In situ high-energy XRD

We applied synchrotron X-ray diffraction to determine the thermal expansion of Al and Cu during the overcharge abuse and normal charge of 18650 cells. High-energy synchrotron X-rays have the unique capability to penetrate the battery case and reveal structural changes in materials under realistic conditions. The results can be used to track the exothermic events at both the cathode and anode.

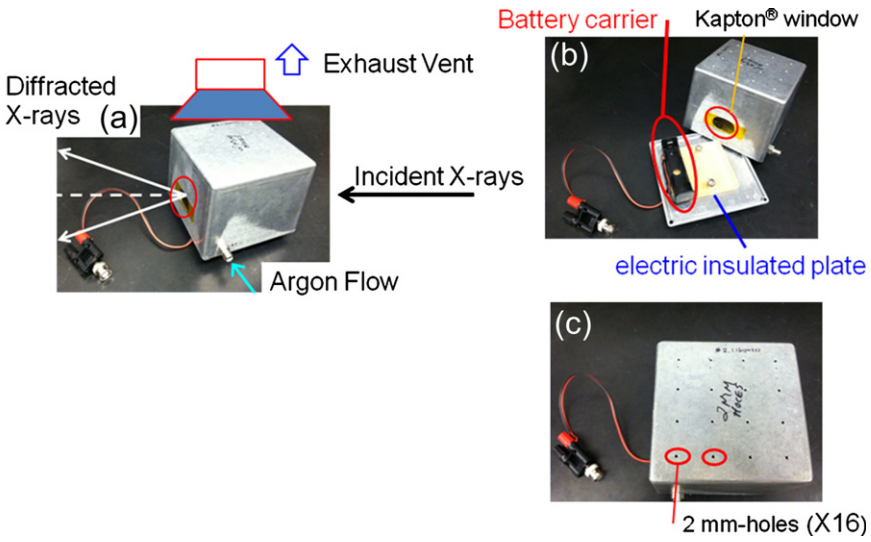

Fig. 2. A safety guard for overcharged 18650 lithium-ion batteries for *in situ* XRD. (a) Overview of the safety guard. (b) Inner view of the safety stainless-steel box. (c) Top-side view of the box.

In situ XRD spectra were collected on beam line 11-ID-C of the Advanced Photon Source (APS) at Argonne National Laboratory. A 115-keV X-ray source with a wavelength of 0.10804 Å was used to study materials inside the 18650 cells. The cells were placed in the X-ray beam of the XRD spectrometer, and diffraction data were collected during electrochemical testing of the batteries. Each XRD scan was collected within 1 min to maintain a good signal-to-noise ratio, and the data in the whole 2θ-range of 0.3–8° (corresponding to 4–114° with wavelength 1.54 Å) were simultaneously collected by an amorphous silicon detector (2-D Perkin Elmer). The reduced data collection time for each scan allowed us to study thermal variation in real time. Furthermore, the synchrotron light source has a low spatial distribution, providing high resolution for the lattice expansion study.

The overcharge tests were carried out on 18650 cells discharged at a C/3 (0.5 A) constant current without a compliance (upper cut-off) voltage. These 18650 cells have an internal current-interrupt device (CID), which is triggered by internal pressure build-up. Once gases are produced from electrode degradation or electrolyte decomposition during the overcharge, the internal pressure of the cell increases, and the current is interrupted internally. Therefore, the cell neither ruptures nor catches fire.

2.4. Standard curve for temperature vs. lattice constant of Al and Cu

It is well known that the cell parameters of crystalline materials increase proportionally to the increase of external temperature; hence, the local temperature of the environment can be measured by detecting the cell parameters of crystalline materials such as copper or aluminum [22,23]. To obtain a reliable reference for the temperature variation reported in this work, we stacked several pieces of Al or Cu foils together and heated the stack in a Linkam THMS600 heating and freezing stage, which promises 0.1 °C accuracy and stability. The metal foils were heated to set points and kept at the selected temperature for 30 min to make sure that the whole system reached its thermal equilibrium before XRD measurement. The lattice constants of Al and Cu were determined by Rietveld refinement by means of the GSAS suite of programs [24] (Both Al and Cu possess a cubic lattice with a space group of Fm3m.). The obtained lattice constants of Al and Cu are plotted as function of the exposed temperature in Fig. 3, which indicates that the lattice constants vary linearly with temperature.

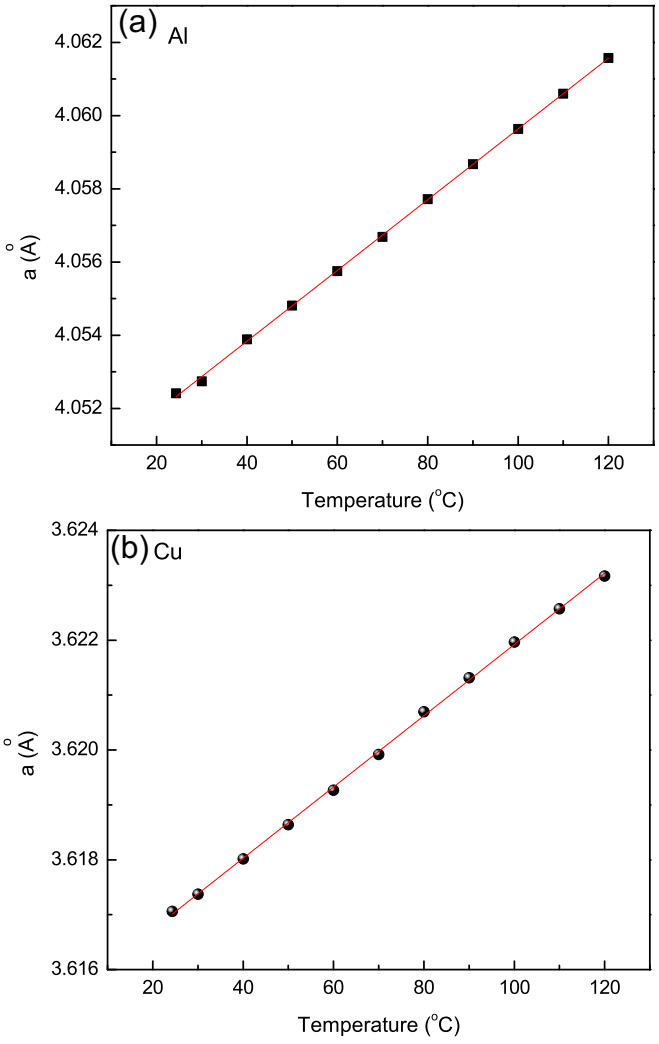

Fig. 3. Lattice constants of Al (a) and Cu (b) *versus* temperature. The two parameters have a linear relationship in this temperature range. Estimated standard deviations are much smaller than symbol sizes.

3. Results and discussion

Fig. 4 shows the continuous *in situ* XRD scans for an 18650 cell that is charged from 3.5 V with a C/3 (0.5 A) constant current until the charge current is interrupted by the internal CID, which is triggered by overcharge abuse. As shown in Fig. 4b, the charge current is interrupted at 5.2 V, after which the voltage of the cell decreases. Of the 294 XRD scans obtained (one every minute), 59 are plotted in Fig. 4a in the 2θ region of 1–5.2° to illustrate the structural evolution of the cathode, anode, and current collectors, as well as the container (α-Fe). The plot shows the XRD scans stacked, each offset to its corresponding position on the electrochemical curve (Fig. 4b).

The reflections for NCA are indexed to hexagonal phases (H1, H2, and H3) similar to those reported by Yoon et al. for $Li(Ni_{0.8}Co_{0.15}Al_{0.05})O_2$ [25], which indicate the structural behavior of the cathode. Because the 18650 cell is not in its first charge cycle, there is no peak splitting of NCA as it undergoes the H1-to-H2 phase transition. At the same time, the featured reflections of Li-inserted graphite occur at around 1.8°, indicating the phase transition of the anode [26]. Most important, there are distinguishable reflections of the Al and Cu foils, which can be used as an indicator of the temperature variation. The lattice constants of Al and Cu can represent the temperature of the cathode and anode for these reasons:

1) Neither Al nor Cu is involved in lithiation or delithiation reactions [27]. Thus, the lattice expansions of Al and Cu are mainly due to their respective thermal expansions.
2) Both Al and Cu have good electric conductivity ($3.65 \times 10^7\ \Omega^{-1}$ for Al and $5.88 \times 10^7\ \Omega^{-1}\ m^{-1}$ for Cu) [28]. Due to the low resistivity (R), the resistive heating (I^2R) of Al and Cu under constant current is invariant and negligible.
3) Moreover, the lattice constants of Al and Cu vary linearly with temperature, making it reliable to estimate the temperature from their lattice constants (see Fig. 3).
4) The contribution of either internal pressure of 18650 cells or stress of electrodes to the lattice expansions of Cu and Al is estimated less than 1%.

Rietveld structural refinement of the *in situ* XRD data allows us to obtain the lattice constants of Al and Cu foils. The process is similar to that for obtaining the standard temperature curve of Al and Cu foils. However, for *in situ* XRD, the delithiated cathode material (NCA) is also included to deal with the overlapping of several diffraction peaks from the cathode and Al foil. One refinement result is shown in Fig. 5 as an example. The 2θ angle regions of 1–5.2° are used for all Rietveld refinements, with the regions of the anode and α-Fe case reflections excluded.

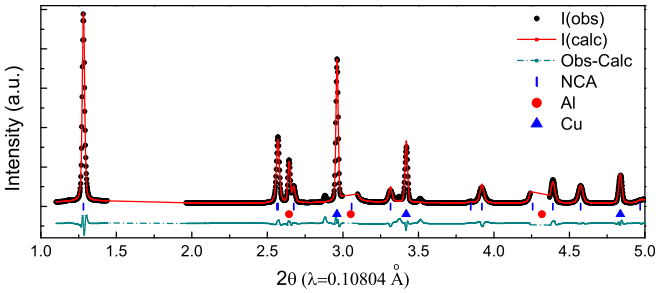

Fig. 5. Reviled refinement profile of *in situ* XRD collected at 4.0 V. The black points indicate observed data, the red solid line shows the calculated diffraction pattern, and the lower dark cyan line is the difference. The reflection markers of blue bars, red circles, and blue triangles belong to NCA, Al, and Cu, respectively. The agreement between the observation and the calculation is estimated by the following indicators: $Rw = 0.10$, $Rp = 0.06$ and $\chi^2 = 7.453$ for 27 variables. (For interpretation of the references to colour in this figure legend, the reader is referred to the web version of this article.)

The lattice constants of Al and Cu for the cell during overcharge are translated into temperature by using the reference curves in Fig. 3. The temperature difference profiles of Al and Cu are associated with the potential curve of the 18650 cell (open black circles) to represent the occurrence of exothermic reactions at the cathode or anode and the charge state (Fig. 6). The voltage drop at the end of the overcharge is mainly ascribed to structural relaxation of electrodes [29] and reduced polarization [30] as a result of charge current interrupted by the CID activation.

The temperature curve of the cathode (Fig. 6b) includes two blank rectangles. That is because the (111) reflection of Al is overlapped by the (012) reflection of NCA at the beginning of charge and is interfered with by the (006) reflection of NCA in the capacity interval of 1600 mAh–2000 mAh (see supporting information, Fig. S1).

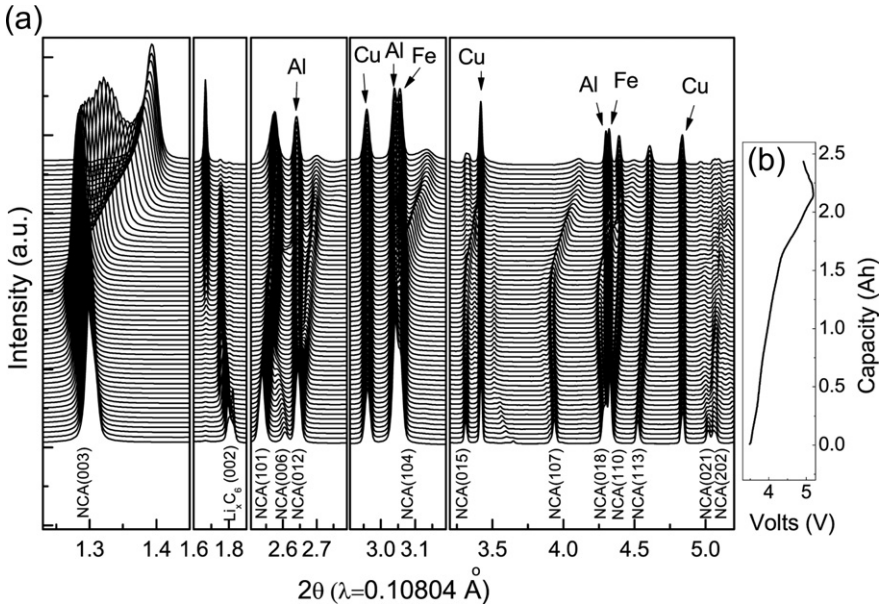

Fig. 4. (a) *In situ* XRD patterns and (b) the electrochemical curve of MCMB/NCA 18650 lithium-ion cell undergoing normal charge and overcharge abuse.

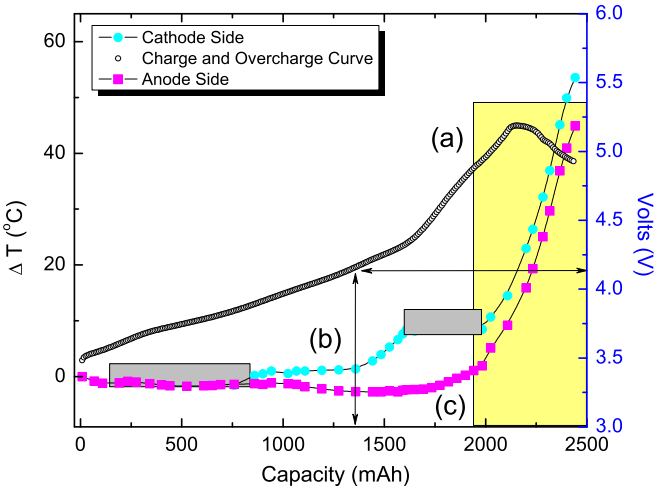

Fig. 6. Temperature variation of cathode and anode in the 18650 cell during a charge and overcharge cycle. (a) The electrochemical curve. The *y*-axis at the right denotes the voltage of the 18650 cell. The *x*-axis denotes the capacity (mAh) that the cell was charged to as the XRD was taken. (b) Temperatures of the cathode current collector, Al. The *y*-axis at the left indicates the temperature difference. The temperatures are estimated from the thermal expansion of Al foils. The two blank regions (with capacity below 835 mAh and between 1600 and 2000 mAh) are due to the overlapping of Al by NCA peaks. (c) Temperatures of the anode current collector, Cu. (For interpretation of the references to colour in this figure legend, the reader is referred to the web version of this article.)

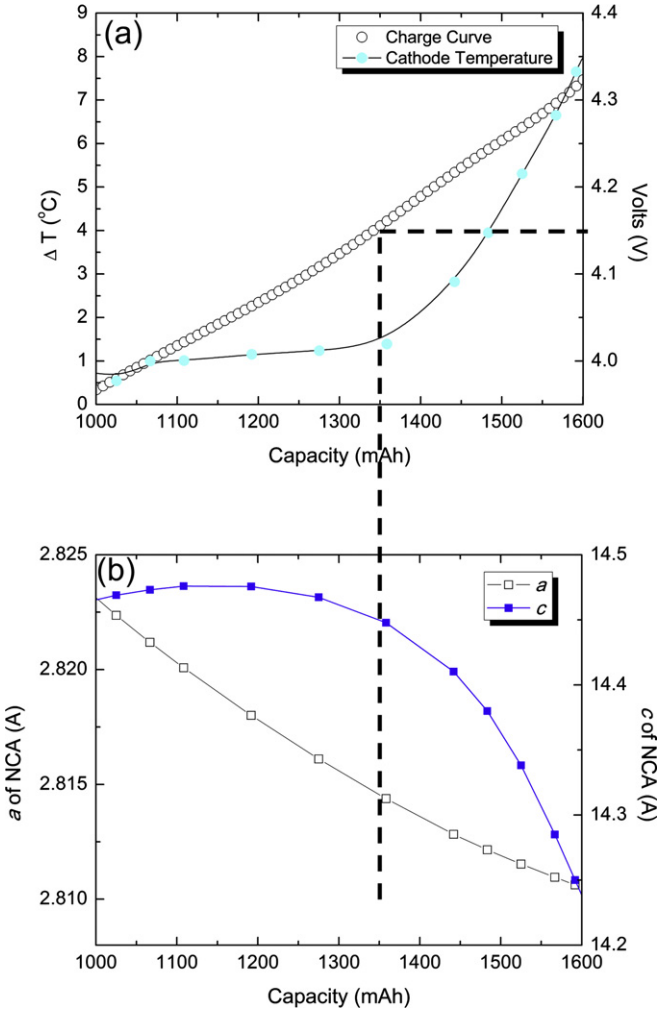

Fig. 7. (a) Voltage profile of cell (open circle) and temperature profile of cathode (closed circle). (b) Lattice parameters *a* and *c* for NCA as determined by Rietveld refinement. Estimated standard deviations are smaller than symbol size. The dashed line denotes the exothermic reaction.

Fig. 6 shows that the temperature profile of the cathode is different from that of the anode in an overcharged lithium-ion cell, indicating that measurable exothermic reactions first occur on the cathode side. The line with the cyan-colored symbols (closed circles) shows that the exothermic process started on the cathode side as the cell is charged to around 1.35 Ah (2.7 h) and the voltage approaches 4.16 V, followed by a stronger exothermic reaction at a higher voltage.

The *in situ* XRD plots (Fig. 4) show that the exothermic reaction at 4.16 V is related to a dramatic structural change of the cathode material. When the cathode material first experiences an exothermic reaction, it also undergoes an H2-to-H3 phase transition, shown by the shift of the NCA (003) peak to a larger 2θ value. Further structural refinement reveals that lattice constants *a* and *c* shrink as the voltage of the cathode increases (Fig. 7). The cathode material possesses layer structure along *c*-axis and the lattice structure can be illustrated as lithium ion intercalated in $Ni_{0.8}Co_{0.15}Al_{0.05}O_2$ sheets. As the battery undergoes charging, lithium ion is continually extracted from the structure and the *c* parameter increases initially due to an increasing electrostatic repulsion between adjacent $Ni_{0.8}Co_{0.15}Al_{0.05}O_2$ sheets. The *a* parameter decreases initially with decreasing lithium content due to the reduced ion radii of Ni and Co with increase in the oxidation state. When lithium ions are continually extracted from the layer structure of the host material, the electrostatic repulsion of the oxygen anions increases until a gliding occurs to release the stress [31,32]. The slight increase in temperature (0.5 °C) before the cell is charged for 1.35 Ah is ascribed to resistive heating, since a constant current of 0.5 A is applied to the cell. As the battery is charged to an even higher voltage, diffraction peaks of the cathode shift to larger 2θ. This behavior means that the overcharge keeps extracting lithium ions from the cathode.

The voltage profile between 4.4 V and 5.2 V in Fig. 6 (corresponding to capacities of 1650 mAh–2100 mAh) also suggests oxidation reaction induced by overcharge. It has been reported that half cells using NCA as the cathode exhibit a similar potential profile in the overcharge region [33]. Therefore, the continuing temperature elevation on the cathode side between 4.4 V and 5.2 V may be due to the oxidation of the electrolyte on the surface of the highly delithiated cathode. Because the capacity of the anode is greater than that of the cathode in the 18650 cell (ratio of 1.2), the cathode material becomes unstable and reacts with the electrolyte at high voltage, while the anode still works normally with extra capacity to host more lithium.

In Fig. 6, the line with the magenta-colored symbols (closed squares) shows the temperature variation at the anode. From 0 to 1500 mAh (3.5 h), the thermal expansion of Cu indicates that the anode temperature slightly decreases. This finding is somewhat at variance with conventional wisdom for charged cells. When external electric energy is injected into the cells, part of the electrical energy is transferred to electrochemical potential, and some is lost as waste heat. However, endothermic events in cells with graphite anodes during the charge are supported by many calorimetric measurements, and they can be attributed to positive entropy change as the lithium-inserted graphite structure changes from order to disorder during the charge [11,34]. From 1500 mAh to 1920 mAh, in our tests, the anode temperature curve changes back to zero from a negative value. This behavior may indicate that there are no endothermic events in this range, and the cell temperature is at equilibrium with the environment.

Temperature elevation of the anode occurs as the capacity of cell arrives at 1920 mAh, and the cell voltage approaches 4.85 V (shaded region on far right of Fig. 6). The 18650 cell has a reversible capacity of 1600 mAh and an anode-to-cathode capacity ratio of 1.2. Thus, when the capacity enters the shaded region, the graphite anode reaches 100% saturation by lithium insertion. As the graphite then has no space to host extra lithium, the lithium is deposited on the anode surface as lithium metal. The resulting dramatic temperature increase of the anode may be due to the reaction between the deposited lithium metal and the non-aqueous electrolyte.

4. Conclusions

We demonstrated that *in situ* high-energy XRD can be a powerful technique to study the contribution of anodes and cathodes in the failure mechanism of lithium-ion batteries. The lattice expansion of current collectors — Al on the cathode side and Cu on the anode side — was investigated by *in situ* XRD to estimate the local temperature inside the 18650 cells. This new approach enabled us to discriminate the temperature of the cathode from that of the anode as the battery underwent overcharge abuse. The temperature of the cathode increased first as the cell voltage reached 4.16 V, and the increase in temperature continued with increasing voltage. In contrast, the temperature of the anode decreased slowly during the initial portion of the charging process and increased only when the cell was charged above 4.58 V. The difference in the temperature profile between the cathode and the anode suggests that the electrochemical stability of the delithiated cathode plays a more critical role than the anode in the specific chemistry studied here. A cathode material with better electrochemical stability may have better tolerance toward overcharge abuse.

Acknowledgments

Research at Argonne National Laboratory was funded by U.S. Department of Energy, FreedomCAR and Vehicle Technologies Office. Argonne National Laboratory is operated for the U.S. Department of Energy by UChicago Argonne, LLC, under contract DE-AC02-06CH11357. The authors also acknowledge the use of the Advanced Photon Source of Argonne National Laboratory supported by the U.S. Department of Energy, Office of Science, Office of Basic Energy Sciences.

Appendix A. Supplementary data

Supplementary data related to this article can be found at http://dx.doi.org/10.1016/j.jpowsour.2012.12.032.

References

[1] T.H. Bradley, A.A. Frank, Renew. Sust. Energ. Rev. 13 (2009) 115–128.
[2] B. Dunn, H. Kamath, J.-M. Tarascon, Science 334 (2011) 928–935.
[3] Z. Chen, Y. Qin, Y. Ren, W. Lu, C. Orendorff, E.P. Roth, K. Amine, Energy Environ. Sci. 4 (2011) 4023–4030.
[4] Z. Chen, Y. Qin, J. Liu, K. Amine, Electrochem. Solid-State Lett. 12 (2009) A69–A72.
[5] K. Amine, Z. Chen, Z. Zhang, J. Liu, W. Lu, Y. Qin, J. Lu, L. Curtis, Y.-K. Sun, J. Mater. Chem. 21 (2011) 17754–17759.
[6] I. Belharouak, D. Vissers, K. Amine, J. Electrochem. Soc. 153 (2006) A2030–A2035.
[7] F. Torabi, V. Esfahanian, J. Electrochem. Soc. 158 (2011) A850–A858.
[8] A. Hammami, N. Raymond, M. Armand, Nature 424 (2003) 635–636.
[9] Q. Wang, P. Ping, X. Zhao, G. Chu, J. Sun, C. Chen, J. Power Sources 208 (2012) 210–224.
[10] Y. Saito, K. Takano, A. Negishi, J. Power Sources 97–98 (2001) 693–696.
[11] W. Lu, J. Prakash, J. Electrochem. Soc. 150 (2003) A262–A266.
[12] S.-I. Tobishima, J.-I. Yamaki, J. Power Sources 81–82 (1999) 882–886.
[13] R. Spotnitz, J. Franklin, J. Power Sources 113 (2003) 81–100.
[14] R.A. Leising, M.J. Palazzo, E.S. Takeuchi, K.J. Takeuchi, J. Electrochem. Soc. 148 (2001) A838–A844.
[15] C. Forgez, D. Vinh Do, G. Friedrich, M. Morcrette, C. Delacourt, J. Power Sources 195 (2010) 2961–2968.
[16] R. Srinivasan, J. Power Sources 198 (2012) 351–358.
[17] Q. Wang, J. Sun, X. Yao, C. Chen, J. Electrochem. Soc. 153 (2006) A329–A333.
[18] D. Belov, M.-H. Yang, J. Solid State Electrochem. 12 (2008) 885–894.
[19] R.A. Leising, M.J. Palazzo, E.S. Takeuchi, K.J. Takeuchi, J. Power Sources 97–98 (2001) 681–683.
[20] C.-H. Doh, D.-H. Kim, H.-S. Kim, H.-M. Shin, Y.-D. Jeong, S.-I. Moon, B.-S. Jin, S.W. Eom, H.-S. Kim, K.-W. Kim, D.-H. Oh, A. Veluchamy, J. Power Sources 175 (2008) 881–885.
[21] T. Ohsaki, T. Kishi, T. Kuboki, N. Takami, N. Shimura, Y. Sato, M. Sekino, A. Satoh, J. Power Sources 146 (2005) 97–100.
[22] C.Y. Ho, R.E. Taylor, Thermal Expansion of Solids, ASM International, Materials Park, OH, 1998.
[23] M.E. Straumanis, L.S. Yu, Acta Crystallogr., Sect. A: Found. Crystallogr. A25 (1969) 676–682.
[24] A.C. Larson, R.B. Von Dreele, Los Alamos National Laboratory Report LAUR (2004). pp. 86–748.
[25] W.-S. Yoon, K.Y. Chung, J. McBreen, D.A. Fischer, X.-Q. Yang, J. Power Sources 174 (2007) 1015–1020.
[26] J.R. Dahn, Phys. Rev. B 44 (1991) 9170–9177.
[27] K. Kanamura, W. Hoshikawa, T. Umegaki, J. Electrochem. Soc. 149 (2002) A339–A345.
[28] G.T. Meaden, Electrical Resistance of Metals, Plenum Press, New York, 1965.
[29] S. Park, M. Oda, T. Yao, Solid State Ionics 203 (2011) 29–32.
[30] K.B. Oldham, J.C. Myland, A.M. Bond, Electrode polarization, in: Electrochemical Science and Technology: Fundamentals and Applications, John Wiley & Sons, Ltd., Chichester, Hoboken, Toronto, 2011, pp. 193–212.
[31] J.M. Tarascon, G. Vaughan, Y. Chabre, L. Seguin, M. Anne, P. Strobel, G. Amatucci, J. Solid State Chem. 147 (1999) 410–420.
[32] J.-S. Hong, H. Maleki, S.A. Hallaj, L. Redey, J.R. Selman, J. Electrochem. Soc. 145 (1998) 1489–1501.
[33] T. Sasaki, V. Godbole, Y. Takeuchi, Y. Ukyo, P. Novak, J. Electrochem. Soc. 158 (2011) A1214–A1219.
[34] R. Yazami, Y. Reynier, J. Power Sources 153 (2006) 312–318.

Glossary

CID: current-interrupt device
NCA: $Li_{1-x}Ni_{0.8}Co_{0.15}Al_{0.05}O_2$
SEI: solid–electrolyte interface
XRD: X-ray diffraction